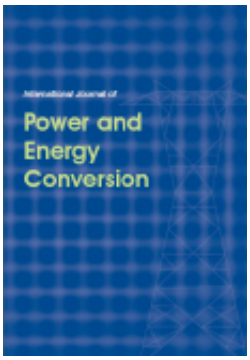

International Journal of Power and Energy Conversion

ISSN online: 1757-1162 - ISSN print: 1757-1154
https://www.inderscience.com/ijpec

Six-phase DFIG-MPPT synergy: pioneering approaches for maximising energy yield in wind energy generation system

Neeraj Kumar Mishra, Gourav Mishra, Manoj Kumar Shukla

DOI: 10.1504/IJPEC.2024.10062396

Article History:

Received:	12 June 2023
Last revised:	04 September 2023
Accepted:	15 November 2023
Published online:	22 February 2024

Six-phase DFIG-MPPT synergy: pioneering approaches for maximising energy yield in wind energy generation system

Neeraj Kumar Mishra*

Department of Electronics and Electrical Engineering,
NIMS University,
Jaipur, Rajasthan, India
Email: 99neer@gmail.com
*Corresponding author

Gourav Mishra

Department of Electronics and Communication Engineering,
Sagar Institute of Research and Technology,
Bhopal, India
Email: gouravmishra426@gmail.com

Manoj Kumar Shukla

Department of Robotics and Automation,
Symbiosis Institute of Technology,
Symbiosis International (Deemed University),
Pune, India
Email: acdcmks@gmail.com

Abstract: This work is motivated by the issue, 'If a 6-phase doubly fed induction generator (6-phase DFIG) based wind energy generation system (WEGS) will supply power to society in the future, then what type of MPPT system will be appropriate for a 6-phase DFIG-based wind energy generation system?'. The maximum power point tracking (MPPT) technique has been adopted to obtain maximum power under various operating situations using a machine-side converter (MSC) linked to a traditional doubly fed induction generator (DFIG) and solar photovoltaic cells throughout the last several decades. Due to several two-dimensional space harmonics, the MPPT technique to the MSC of 6-phase DFIG cannot be applied directly, and as a result 6-phase DFIG modelling is first introduced in a distinct two-dimensional plane. An appropriate MPPT algorithm has been developed based on the proposed modelling that provides the synergy between the 6-phase DFIG and MPPT system. In addition, the modelling of a WEGS is also covered in this study, along with the modelling of a 6-phase transformer, a DC link capacitance, and a wind turbine. Furthermore, real-time hardware-in-loop experimentation has been conducted to validate the efficacy of the proposed model.

Keywords: 6-phase DFIG-MPPT synergy; 6-phase DFIG; machine-side converter; maximum power point tracking.

Reference to this paper should be made as follows: Mishra, N.K., Mishra, G. and Shukla, M.K. (2024) 'Six-phase DFIG-MPPT synergy: pioneering approaches for maximising energy yield in wind energy generation system', *Int. J. Power and Energy Conversion*, Vol. 15, No. 1, pp.79–98.

Biographical notes: Neeraj Kumar Mishra received his BE (Electrical Engineering) and ME (Measurement and Control) from the Madhav Institute of Technology and Science Gwalior, India, in 2007 and 2011, respectively, and his PhD from the National Institute of Technology Hamirpur, India in 2022. He has worked as a faculty member at various reputed institutes like NIT Hmirpur, NIT Delhi, etc. With a passion for teaching and an unwavering commitment to research, he has made significant contributions to the field of 'six-phase doubly fed induction generator' throughout his illustrious career. His areas of interest include power electronics, machines and drives, energy generation, wind energy generation, solar photovoltaic power generation, electric vehicle, AI, and economic load dispatch. Presently, he is working as an Associate Professor in the Department of Electronics and Electrical Engineering at NIMS University Jaipur Rajasthan.

Gourav Mishra graduated from Samrat Ashok Technological Institute (SATI) Vidisha in Electronics and Instrumentation Engineering Course in 2020. Currently, he is pursuing his MTech from RGPV Bhopal. His research interest includes multi-phase electric machines, controlling of conventional machines and multiphase machines, controlling of six-phase doubly fed induction generator, renewable energy resources, power electronics and economic load dispatch.

Manoj Kumar Shukla is currently working as an Assistant Professor in the Department of Robotics and Automation, Symbiosis Institute of Technology, Pune which is a constituent of Symbiosis International (Deemed University), Pune. Prior to that, he worked at Lovely Professional University, Phagwara, Punjab. He completed his MTech and PhD in Electrical Engineering (Control Systems) from NIT, Hamirpur (Himachal Pradesh), India. He has eight years of teaching and research experience. His research interests mainly include control systems, fractional calculus, power systems, renewable energy resources, power electronics, etc.

1 Introduction

The technology is changing very rapidly, and due to the potential success of the doubly fed induction generator (DFIG) in wind energy generation systems (WEGS), the interest of the research fraternity is growing towards the six-phase doubly fed induction generator (6-phase DFIG)-based WEGS. Out of many commercially viable WEGS, 6-phase DFIG-based WEGS becomes the most desirable due to inherent fault tolerance capability (Marques and Iacchetti, 2019; Mishra et al., 2020). The reliability, harmonics mitigation, and reduction of per phase current in stator windings of 6-phase DFIG is advanced compared to the three-phase DFIG, and hence, the quality of power in WEGS will improve (Mishra and Husain, 2023; Sridhar et al., 2015). The frequency and voltage generated by the DFIG can fluctuate during power generation due to the erratic behaviour of the wind. The maximum power point tracking (MPPT)-based control strategy of 6-phase DFIG plays a vital role in improving WEGS efficiency (Arevalo et al., 2019;

Yang et al., 2017). A good number of articles have been published on MPPT techniques for conventional DFIG, but 6-phase DFIG-MPPT Synergy has yet to be reported anywhere in the world as per information of Kazmi et al. (2010b).

The DFIG-MPPT synergy is widely used due to its maximum power extraction capability. The pitch angle and tip speed ratio play a vital role in maximum extraction from WEGS. As a result, in the MPPT technique, the calibration of tip speed ratio and pitch angle is a critical factor. To generate most of the available power, the power coefficient must be optimal as well as constant while the speed of the wind turbine (WT) varies. The MPPT not only increases efficiency but also lowers installation costs, and supplies reactive power on demand (Kumar and Chatterjee, 2016; Calderaro et al., 2008).

In the current scenario, soft computing and traditional method-based MPPT algorithms have been developed for WEGS. Soft computing-based MPPT algorithms have advantages over hardware methods, such as low cost, simple implementation, high performance, and high flexibility. Several authors have used soft computing technologies to achieve optimum power, such as fuzzy logic (Mohamed et al., 2001; Khan and Mathew, 2019b; Tiwari et al., 2018), neural network (Datta and Ranganathan, 2003; Li et al., 2005; Dahri et al., 2023), grouped grey wolf optimisation (Yang et al., 2017), and democratic joint operation (Yang et al., 2018). However, the soft computing method suffers from computational complexity, large computer memory, high processing time, and the professionalism required to investigate these methods at an industry level. On the other hand, the conventional MPPT methods are more dependent on either indirect power control or direct power control. The indirect power controller (IPC) method is appropriate for maximising power using WT power, whereas the direct power controller (DPC) method can directly maximise power. Tip speed ratio (Rathi and Sandhu, 2016), power signal feedback (Yadav et al., 2021), and optimal torque (Abdullah et al., 2012) are the most popular IPC-based MPPT algorithms. Furthermore, DPC-based MPPT algorithms include the hill climb search (HCS) algorithm (Bianchi et al., 2007), the incremental conductance algorithm (ICA) (Kazmi et al., 2010a), and the hybrid algorithm (Khan and Mathew, 2019a). Even though numerous kinds of literature on a three-phase DFIG with an MPPT algorithm is available, the MPPT algorithm for the specific case of 6-phase DFIG requires adequate proficiency. Because 6-phase machines have a large number of stationary spaces harmonic, the procedures used for three-phase WEGS cannot be simply applied to 6-phase DFIG. As a result, there is a significant research gap available for these applications.

1.1 Objective

In reality, any three-phase wound rotor induction machine can be simply converted to a 6-phase machine without the need to cast the stator perimeter and losses due to the slip ring can be reduced by taking three phases of the rotor winding instead of 6-phases on the rotor side.

The following research objectives are identified based on a review of the available literature for 6-phase DFIG modelling.

- to develop 6-phase DFIG-MPPT synergy
- to develop mathematical modelling of 6-phase DFIG
- to develop an MPPT algorithm for 6-phase DFIG-based WEGS.

1.2 Contribution

This paper emphasises the modelling and control of 6-phase DFIG WEGS with the following attributes

- A novel dynamic modelling based on the 6-phase DFIG is proposed for better control of active and reactive power demand by WEGS.
- An appropriate MPPT algorithm is designed to generate an optimal switching signal for 6-phase DFIG converters.
- Rotor power of 6-phase DFIG is also recovered through an additional three-phase MSC followed by 6-phase GSC by utilising the proposed controller.

Section 2 describes the modelling of WEGS, including the structure, connections, interface modelling of 6-phase DFIG, modelling of the WT, and modelling of a six-phase transformer. Section 2 also represents the MPPT and closed-loop control of 6-phase DFIG. Section 3 contains the results and discussion; Section 4 concludes with a future scope for industry and research.

2 Modelling of WEGS

The proposed WEGS has the capability to feed both the three-phase and six-phase grid systems. This WEGS system can generate electric energy by exacting the kinetic energy of wind using various components. The components include a 6-phase DFIG, a six-phase transformer (SPT), a grid side converter (GSC), and a machine side converter (MSC), as shown in Figure 1.

Figure 1 The complete setup of proposed WEGS with three-phase and six-phase grid system (see online version for colours)

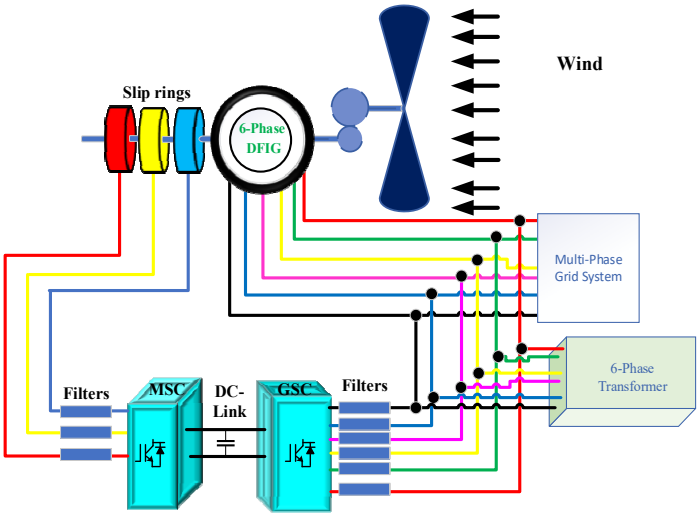

2.1 Modelling of 6-phase DFIG

Figure 2 represents the schematic diagram of 6-phase DFIG-based WEGS. The rotor of this prototype is wound with three-phase windings, while the stator is wound with six-phase windings.

Figure 2 Schematic diagram of six-phase doubly fed induction machine laboratory prototype (see online version for colours)

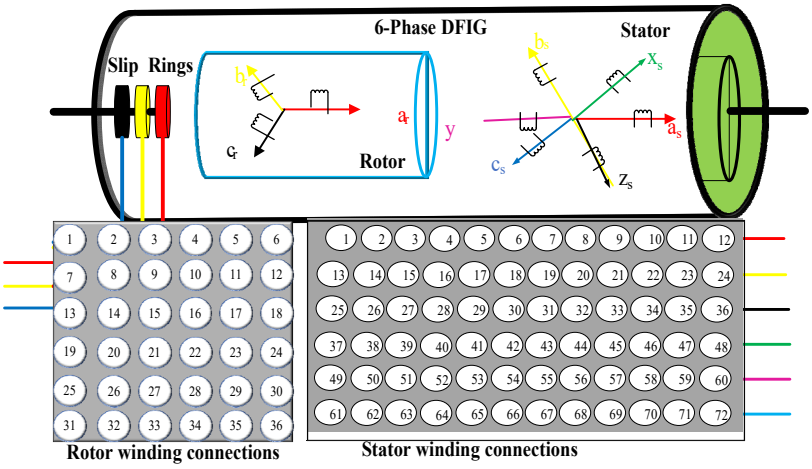

Furthermore, this novel machine has 72 terminals, 36 slots, six poles, and a three-phase split phase belt. To make a six-phase winding arrangement on the stator side, all 72 terminals of the stator coils are mounted on a wooden plate using nuts and bolts outside the machine. To take advantage of the minimal power loss in slip rings, the three-phase rotor windings are chosen for this machine. However, the rotor windings can also be made six-phase for a specific application, as shown in Fig 3. The specifications of the 6-phase DFIG can be illustrated in Table 1.

Table 1 Parameters of 6-phase DFIG

Parameters	*Values*
Number of poles	6
Stator and rotor voltage	415 V, 200 V
Stator and rotor current	12 A, 12 A
Frequency of stator magnetic field	50 Hz
Stator and rotor resistance (r_s, r_r)	1.32 Ω, 1.71 Ω
Stator and rotor leakage inductance (L_{ls}, L_{lr})	6.83 mH, 43.30 mH
Mutual inductance L_m	0.22 mH

The stator of 6-phase DFIG is composed of two sets of star connected three-phase windings with 60° (electrical) phase displacement between two consecutive windings. One set of three-phase windings considers {as, bs, cs} and another set of three-phase windings are represented by {xs, ys, zs}. As a precaution against physical faults and significant current harmonics, the neutral points of the two three-phase sets (star

connection) are kept separate. The phase voltages of GSC and MSC (v_{js} and v_{jr}) can be denoted by (1).

$$v_{js} = r_s i_{js} + \frac{d\psi_{js}}{dt} \quad \text{and} \quad v_{jr} = r_r i_{jr} + \frac{d\psi_{jr}}{dt} \tag{1}$$

where r_s and r_r represent the stator and rotor phase resistances, respectively. ψ_{js} and ψ_{jr} represent the stator and rotor flux linkage of phases $js \in$ {as, bs, cs, xs, ys, zs}and $jr \in$ {ar, br, cr} respectively. Similarly, i_{js} and i_{jr} represent the stator and rotor phasor currents respectively. Directly controlling the instantaneous values of i_{js}, i_{jr}, ψ_{js} and ψ_{jr} are very difficult. Hence, this paper utilises the concept of reference frame theory (Mishra and Husain, 2023). For simple controllability of 6-phase DFIG, the modelling of 6-phase DFIG is illustrated in the dq stator reference frame. The stator reference frame-based voltage relations of the stator and rotor winding can be written as (2).

$$\begin{bmatrix} v_{d1s} \\ v_{q1s} \end{bmatrix} = R_s \begin{bmatrix} i_{d1s} \\ i_{q1s} \end{bmatrix} + \frac{d}{dt} \begin{bmatrix} \psi_{d1s} \\ \psi_{q1s} \end{bmatrix} \tag{2}$$

$$\begin{bmatrix} v_{d2s} \\ v_{q2s} \\ v_{0s^+} \\ v_{0s^-} \end{bmatrix} = R_s \begin{bmatrix} i_{d2s} \\ i_{q2s} \\ i_{0s^+} \\ i_{0s^-} \end{bmatrix} + \frac{d}{dt} \begin{bmatrix} \psi_{d2s} \\ \psi_{q2s} \\ \psi_{0s^+} \\ \psi_{0s^-} \end{bmatrix} \tag{3}$$

$$\begin{bmatrix} v_{dr} \\ v_{qr} \\ v_{0r} \end{bmatrix} = R_s \begin{bmatrix} i_{dr} \\ i_{qr} \\ i_{0r} \end{bmatrix} + \frac{d}{dt} \begin{bmatrix} \psi_{dr} \\ \psi_{qr} \\ \psi_{0r} \end{bmatrix} \tag{4}$$

The flux and inductance matrix of the stator and rotor coil can be written as (5).

$$\begin{bmatrix} \psi_{d1s} \\ \psi_{q1s} \\ \psi_{dr} \\ \psi_{qr} \end{bmatrix} = \begin{bmatrix} L_s & 0 & L_m & 0 \\ 0 & L_s & 0 & L_m \\ L_m & 0 & L_r & 0 \\ 0 & L_m & 0 & L_r \end{bmatrix} \begin{bmatrix} i_{d1s} \\ i_{q1s} \\ i_{dr} \\ i_{qr} \end{bmatrix}$$
$$\begin{bmatrix} \psi_{d2s} \\ \psi_{q2s} \\ \psi_{0s^+} \\ \psi_{0s^-} \end{bmatrix} = \begin{bmatrix} L_{ls} & 0 & 0 & 0 \\ 0 & L_{ls} & 0 & 0 \\ 0 & 0 & L_{ls} & 0 \\ 0 & 0 & 0 & L_{ls} \end{bmatrix} \begin{bmatrix} i_{d2s} \\ i_{q2s} \\ i_{0s^+} \\ i_{0s^-} \end{bmatrix} \tag{5}$$

The self-inductance of the stator and rotor winding can be defined as $L_s = L_{ls} + L_m$ and $L_r = L_{lr} + L_m$, respectively, whereas L_m represents the mutual inductance of 6-phase DFIG. L_{ls} and L_{lr} represent the leakage inductances of the stator and rotor winding, respectively. The active power (P_s), reactive power (Q_s) and torque (T_{em}) developed by 6-phase DFIG can be represented as (6).

$$
\begin{aligned}
P_s &= 1.5\left(v_{d1s}i_{d1s} + v_{q1s}i_{q1s}\right) \\
Q_s &= 1.5\left(v_{q1s}i_{d1s} - v_{d1s}i_{q1s}\right) \\
T_{em} &= \frac{3PL_m}{4L_r}\left(\psi_{dr}i_{q1s} - \psi_{qr}\psi_{d1s}\right)
\end{aligned} \tag{6}
$$

where P represents the number of poles of 6-phase DFIG.

Figure 3 Connection interface between stator and rotor winding (see online version for colours)

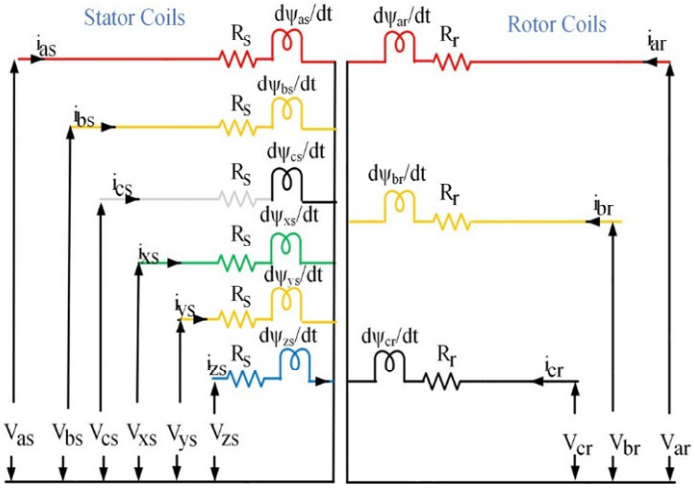

2.2 Modelling of six-phase transformer

Despite the fact that the 6-phase DFIG is capable of the feeding of a six-phase transmission line, the three-phase grid system is so popular in the present day and hence a six-phase transformer can be utilised to feed electric power to the conventional grid. The diagram of the six-phase transformer is shown in Figure 4(a). An illustration depicts the connection diagrams of six phases at the top and the three-phase connections at the bottom. The input and output voltage equations of a six-phase transformer can be expressed as (7).

$$
\begin{bmatrix} v_{ai} \\ v_{xi} \\ v_{bi} \\ v_{yi} \\ v_{ci} \\ v_{zi} \end{bmatrix} = V \begin{bmatrix} \cos(t) \\ \cos\left(t+\frac{\pi}{3}\right) \\ \cos\left(t+\frac{2\pi}{3}\right) \\ \cos(t+\pi) \\ \cos\left(t+\frac{4\pi}{3}\right) \\ \cos\left(t+\frac{5\pi}{3}\right) \end{bmatrix}; \begin{bmatrix} v_{ao} \\ v_{bo} \\ v_{co} \end{bmatrix} = V \begin{bmatrix} \cos(t) \\ \cos\left(t+\frac{2\pi}{3}\right) \\ \cos\left(t+\frac{4\pi}{3}\right) \end{bmatrix} \tag{7}
$$

$$\begin{bmatrix} v_{ao} \\ v_{bo} \\ v_{co} \end{bmatrix} = \begin{bmatrix} 0.5 & 0 & 0 & -0.5 & 0 & 0 \\ 0 & 0 & 0.5 & 0 & 0 & -0.5 \\ 0 & -0.5 & 0 & 0 & 0.5 & 0 \end{bmatrix} \begin{bmatrix} v_{ai} \\ v_{xi} \\ v_{bi} \\ v_{yi} \\ v_{ci} \\ v_{zi} \end{bmatrix} \tag{8}$$

Equation (8) represents the phase transformation relations between the input and output voltages of six-phase transformer.

2.3 Generation of switching signal

Two level voltage source inverters (VSI) are used for both MSC and GSC in the proposed WEGS.

The GSC generates 64 (i.e., 26) switching signal, while the MSC generates only 8 (i.e., 23) switching signals. Generally, an m-level n-phase inverter has $m \times n$ space vectors. The GSC accommodates four null vectors and 60 active vectors, while the MSC utilises two null vectors and six active vectors. In 60 GSC active vectors, 12 are the redundant vectors, which lie along the large vectors. The terminals of inverter leg pole points for six phases and three phases are denoted by $jsi \in$ {ai, bi, ci, xi, yi, zi} and $jri \in$ {ai, bi, ci}, respectively. Moreover, the output phases of the stator and rotor side windings of by 6-phase DFIG are denoted by $js \in$ {as, bs, cs, xs, ys, zs}and $jr \in$ {ar, br, cr}, respectively. The switching frequencies of MSC and GSC are taken as 5 kHz while maintaining the controller sampling frequency of 100 kHz. The phase voltage at the stator of GSC and rotor side of MSC can be realised by (9) and (10), respectively.

$$v_{jsi} = \frac{5}{6} v_{jsi} - \frac{1}{6}\left(\sum v_{jsi} - v_{jsi}\right) \tag{9}$$

$$v_{jri} = \frac{2}{3} v_{jri} - \frac{1}{3}\left(\sum v_{jri} - v_{jri}\right) \tag{10}$$

The grid side switching states are denoted by S_{js}, $\forall j \in$ {a, x, b, y, c, z}, and the condition for gate signal generation is illustrated by Figures 4(b) and 4(c) and machine side switching states are denoted by S_{kr}, $\forall k \in$ {a, b, c}. The GSC and MSC switching states can be written by equations (11) and (12), respectively.

$$v_{js} = \frac{v_{dc}}{6}\left\{5S_{js} - \left(\sum S_{js} - S_{js}\right)\right\} \tag{11}$$

$$v_{jr} = \frac{v_{dc}}{6}\left\{2S_{js} - \left(\sum S_{jr} - S_{jr}\right)\right\} \tag{12}$$

Figure 4 (a) Six-phase transformer connection circuit diagram (b) Representation of switching signal with d_1-q_1 axis (c) Representation of switching signal with d_2-q_2 axis (see online version for colours)

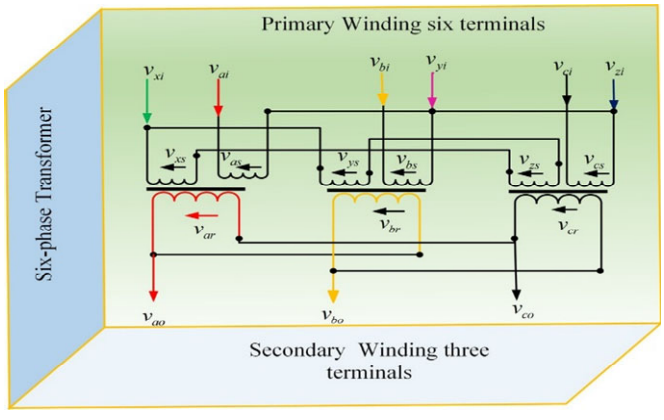

(a)

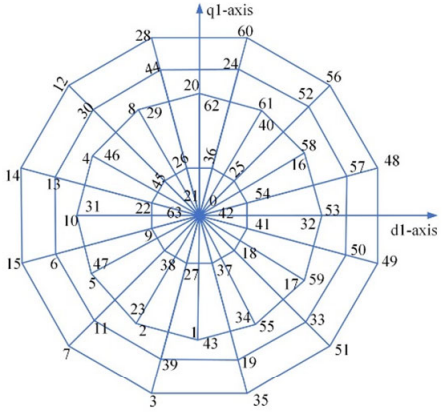

(b)

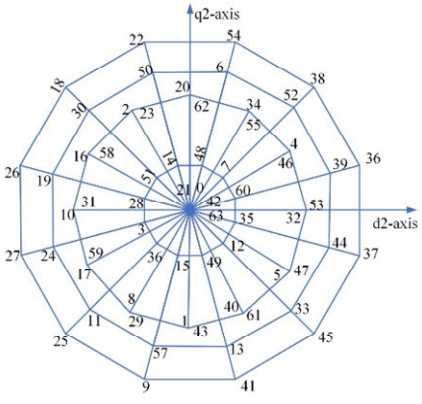

(c)

Figure 5 Performance of wind turbine, (a) $C_p - \lambda$ characteristics of a wind turbine at different pitch angles (b) maximum value of $C_p - \lambda$ characteristics at 0 pitch angle (c) maximum value of $C_t - \lambda$ characteristics at 0 pitch angle (see online version for colours)

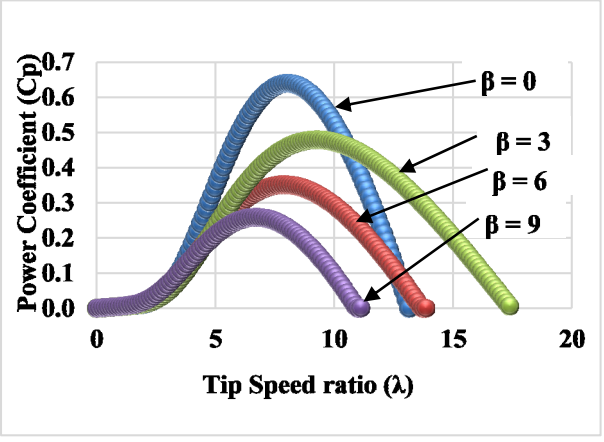

(a)

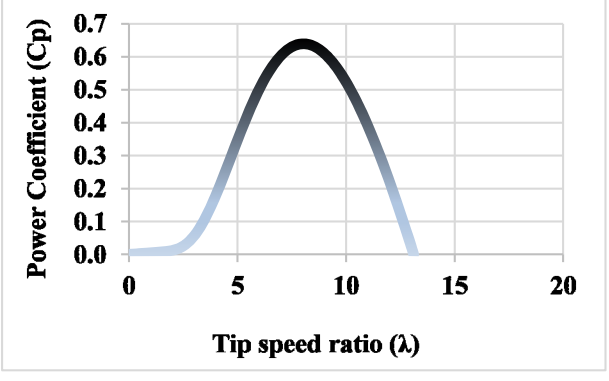

(b)

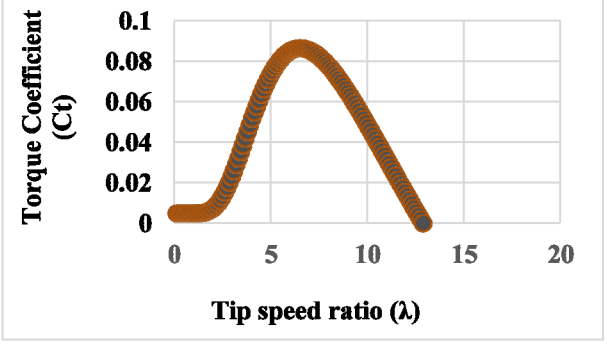

(c)

2.4 Modelling of aerodynamic system

A 6-phase DFIG rotor is powered by the gearbox, which in turn is powered by the blades of a WT turbine. By extracting the energy from moving wind, the kinetic energy developed by the wind can be estimated as (13) (Abad et al., 2011; Koutroulis and Kalaitzakis, 2006; Mishra and Husain, 2019).

$$P_{wind} = \frac{1}{2}\left(\rho \pi R_t^2 v_t^3\right) \tag{13}$$

The actual turbine power received from the kinetic energy of wind is only 59.3%. Hence, only 30 to 40% of kinetic energy can be converted into electrical energy through 6-phase DFIG-based WEGS. The tip speed ratio of WT can be further defined as (14).

$$\lambda_i = \frac{\left(\beta^3 + 1\right)(\lambda + 0.8\beta)}{\left(\beta^3 + 1\right) - 0.35(\lambda + 0.08\beta)}$$

Here $\lambda = \frac{\omega R}{v}$. The complete aerodynamic model of the WT depends on the power coefficient Cp (λ, β), and it is an algebraic function of β and λ.

The equation of power and torque coefficient (Mishra and Husain, 2019) can be written as (15).

$$\begin{aligned} C_p(\lambda, \beta) &= \frac{a_1 a_2}{\lambda_i} - a_1 a_3 \beta - a_1 a_4 e^{\frac{a_5}{\lambda_i} + \frac{a_6}{\lambda_i}} \\ C_t(\lambda, \beta) &= \frac{C_p(\lambda, \beta)}{\lambda_i} \end{aligned} \tag{15}$$

where a_1 = 0.5176, a_2 = 116, a_3 = 0.6, a_4 = 5, a_5 = –21 and a_6 = 0.0068 are the coefficients of $C_p(\lambda, \beta)$.

Table 2 Parameters of 6-phase DFIG

Parameters	*Values*
Rated power	5 kW
Rotor radius	3.2 m
Swept area	32.17 m
Air density	1.225
Cut in speed	<3 m/sec
Cut out speed	>25 m/sec
Survivable wind speed	50 m/sec

Figure 5 represents the performance of the wind turbine. Based on equation (15), the power coefficient versus tip speed ratio curves at different pitch angles and speed are shown in Figure 5(a). Figure 5(b) represents the maximum value of power coefficient $C_p(\lambda, \beta)$ characteristics at 0 pitch angle, and the maximum value of torque coefficient $C_t(\lambda, \beta)$ characteristics at 0 pitch angle can be represented by Figure 5(c). The relation between WT power (mechanical) and power coefficient can be calculated by (16).

$$P_m = \frac{\pi}{2}\rho R^2 v^3 C_p(\lambda, \beta) \tag{16}$$

The parameters of WT aerodynamics can be illustrated by Table 2.

2.5 Maximum power point tracking algorithm

Usually, the MPPT control technique produces better results in low wind speed mode, while the pitch angle control technique produces better results in synchronous speed mode. However, due to the unpredictable nature of wind, obtaining MPPT at a fixed speed is difficult. This led to the development of a variable frequency WT. It is essential to ensure that the WT is controlled to provide the maximum power output to maintain the monotonic nature of MPPT. The DPC-based MPPT technique is illustrated in Arevalo et al. (2019) to generate per-phase electrical power for lossless 6-phase DFIG and can be represented by $P_j = v_{as}i_{as}$. Furthermore, the mechanical power for lossless 6-phase DFIG can be written as $P_m = \omega_m T_m$. The relation between mechanical speed (ω_m) and electrical speed (ω_e) can be written as (17)

$$\omega_m = \frac{v_{as}i_{as}}{T_m} \tag{17}$$

Now, the per-phase electrical power can be modified as (18) using fundamental electromechanical relations and the maximum power can be achieved by solving (19)

$$P_j = v_{as}i_{as} = \frac{ki_f\omega_e}{R_a}v_a - kI_f\omega_e \tag{18}$$

$$\frac{dP_j}{dt} = 0 \tag{19}$$

A change in the DC bus voltage (v_{dc}) proportionately changes the per-phase voltage of the 6-phase DFIG. The DC link in this configuration attempts to maintain a constant voltage in its terminals and regulate the WT power, which acts as a bridge between the MSC and GSC. To provide an active power flow, v_{dc} must always be higher than the peak grid voltage. The dynamics of the DC-link capacitor C_{dc} can be calculated as (20), which can be utilised to regulate v_{dc}.

$$Cv_{dc}\frac{dv_{dc}}{dt} = P_s + P_r \tag{20}$$

For tracking the maximum power points, the mechanical power of WT can be given by (21).

$$\frac{dP_m}{d\omega_r} = \frac{dP_m}{dv_{dc}}\frac{dv_a}{d\omega_e}\frac{d\omega_e}{d\omega_r} \tag{21}$$

By using (21), the optimum power point can be achieved. When $\frac{dP_m}{d\omega_r} = 0$ and $\frac{dP_m}{dv_{dc}} = 0$.

It can be observed that the maximum mechanical power does not depend on the environmental conditions like wind direction and speed. The flow chart of the MPPT algorithm is depicted in Figure 6. The description of the DPC-based MPPT technique is arranged as follows:

Step 1 Set an arbitrary DC side reference voltage V_{ref} for initialisation of the maximum power search method.

Step 2 Measure DC voltage v_{dc} and current i_{dc} at MSC DC-side terminals and calculate electric power.

Step 3 Increase reference voltage V_{dc} using $V_{ref}(k) = V_{ref}(k-1) + \Delta V_{dc}$.

Step 4 Calculate DC power using $P(k) = I_{dc}(k)V_{dc}(k)$.

Step 5 At any wind speed, the four conditions must be met for searching maximum power.

Step 6 $P(K) \geq P(K-1)$ and $V_{dc}(k) \geq V_{dc}(k-1)$ then increase $V_{ref}(k)$ by ΔV_{dc}.

Step 7 $P(K) \geq P(K-1)$ and $V_{dc}(k) < V_{dc}(k-1)$ then decrease $V_{ref}(k)$ by ΔV_{dc}.

Step 8 $P(K) < P(K-1)$ and $V_{dc}(k) \geq V_{dc}(k-1)$ then decrease $V_{ref}(k)$ by ΔV_{dc}.

Step 9 $P(K) < P(K-1)$ and $V_{dc}(k) < V_{dc}(k-1)$ then increase $V_{ref}(k)$ by ΔV_{dc}.

The MPPT characteristics of wind turbine power at three different wind speed V_1, V_2, V_3 are shown in Figure 7. Moreover, the MPPT algorithm (as given in Figure 6) is used for getting the trajectory as indicated by the arrows in Figure 7.

Figure 6 MPPT algorithm flowchart (see online version for colours)

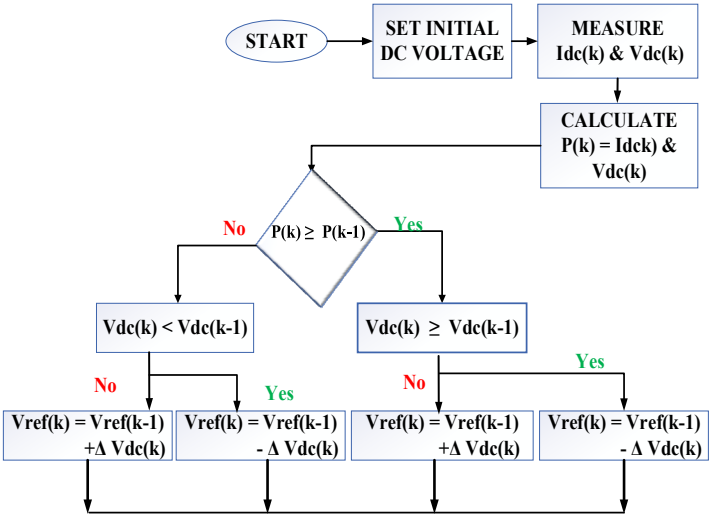

Figure 7 MPPT characteristics (see online version for colours)

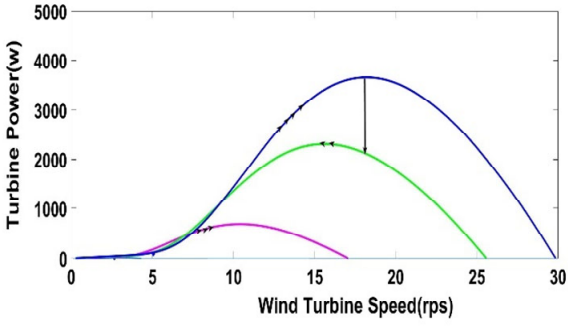

3 Results and discussion

To validate the feasibility of 6-phase DFIG with WT aerodynamics, the corresponding models are emulated using the OP5700 OPAL-RT real-time emulator, as shown in Figure 8. Various outputs such as mechanical power developed by a WT at variable wind velocity, WT power at maximum power points is investigated. Besides, the performances such as stator voltages, stator currents, rotor currents, torque characteristics of WT 6-phase DFIG speed characteristics, grid side active, and reactive power are verified through the real-time emulation. In terms of the WT's mechanical power, it can only be developed within a specific range of wind speeds constrained by cut-in and cut-out speeds. Within these limits, the WT and generator are controlled, and if they exceed this limit, the WT and generator should be shut down for safety reasons. The characteristics of mechanical power developed by wind turbines at various wind speeds are depicted in Figure 9. The plus (+) sign denotes the maximum value of wind turbine power generated (developed at various wind speeds).

Figure 8 OP5700 OPAL-RT prototype for operation of 6-phase DFIG (see online version for colours)

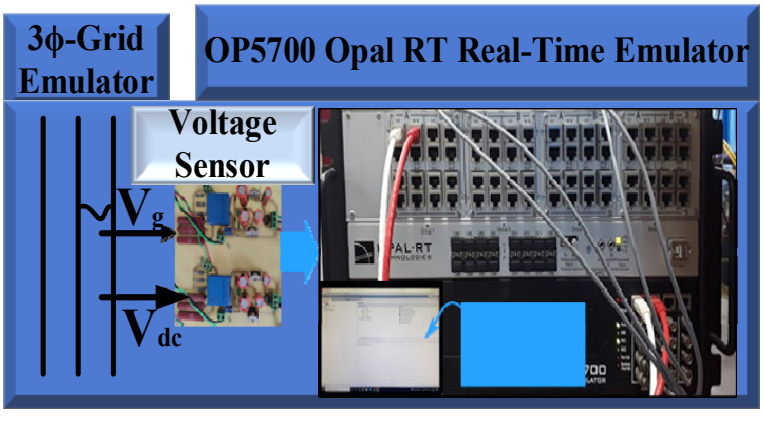

Figure 9 Power developed by wind turbine at wind velocity at variable speed of wind (see online version for colours)

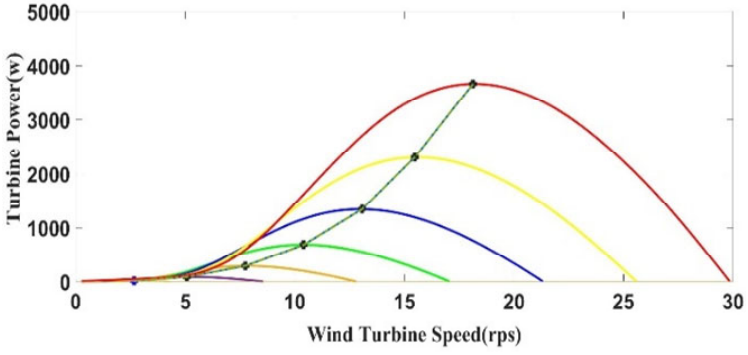

The turbine power generated at different wind speed is illustrated by Figure 9. The developed power at 5 ms^{-1} is close to zero watts, as shown in Figure 9. The golden colour represents the characteristics of the wind turbine at 12 ms^{-1} while the green colour represents the characteristics of wind turbine power at 18 m/sec. Similarly, the characteristics of wind turbine power at various wind speeds are represented by the colours blue, yellow, and red. Figure 10 shows the maximum power developed by the WT at a 0° pitch angle and the maximum power output is around 4000 watts at a speed of about 18 ms^{-1}. Figure 11 depicts the behaviour of a wind turbine's generated power over a range of wind speeds. In Figure 11, the four regions R1, R2, R3 and R4 were used to illustrate the divisions. Region R1 is known as cut-in region if the wind speed varies between 0 ms^{-1} and 3 ms^{-1}. Region R4 is known as cut-out region when the wind speed exceeds 25 ms^{-1}. The power generated by a wind turbine is zero when it is situated in a cut-in and cut-out region. Regions R2 and R3 represent the MPPT and rated power, respectively.

Figure 10 Maximum power developed by Wind turbine at 18 ms^{-1} (see online version for colours)

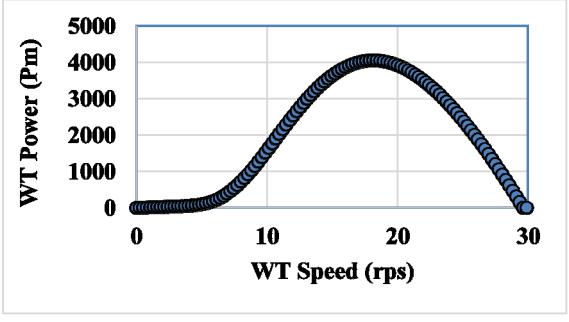

Figure 12 shows the grid side waveforms of voltage and current build-up across a, x, b, y c, z windings. In terms of 6-phase DFIG voltage performance, Figure 12(a) depicts the voltage build-up across a, x, b, y c, z. Furthermore, the phases as, xs, bs, ys, cs, and zs are shown to be displaced at an angle of 0°, 60°, 120°, 180°, 240°, 300° respectively the

output voltage of the stator terminal is 340 volts at 50 Hz frequency. Figure 12(b) shows the grid side current waveforms of 6-phase DFIG.

Figure 11 The characteristics of wind turbine power in R1, R2, R3, R4 region (see online version for colours)

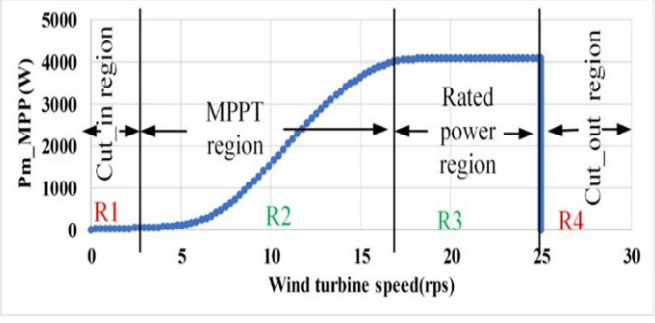

Figure 12 Grid side voltage and current performance of 6-phase DFIG (a)waveforms of voltage winding a, x, b, y, c, z (b) waveforms of current winding a, x, b, y, c, z (see online version for colours)

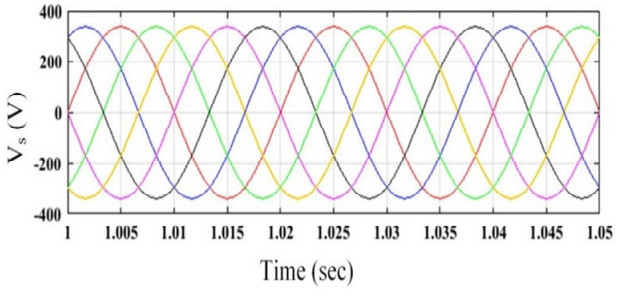

(a)

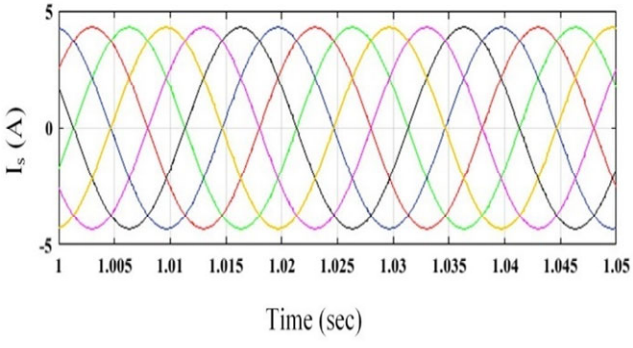

(b)

In a six-phase winding, the phase currents of as, xs, bs, ys, cs, and zs windings are displaced by an angle of 0°, 60°, 120°, 180°, 240°, 300°, respectively.

It can be concluded that 6-phase DFIG is clearly capable of supplying voltage and current to the six-phase grid system, as shown in these waveforms.

Figure 13 depicts the machine side current build-up across the rotor windings (abc) of the proposed 6-phase DFIG. The machine side converter currents in windings ar, br, cr are displaced by an angle of 0°, 120°, 240° because the machine side only has one set of three phase winding.

Figure 13 The current build-up across rotor windings during speed variation from sub synchronous to super synchronous mode (see online version for colours)

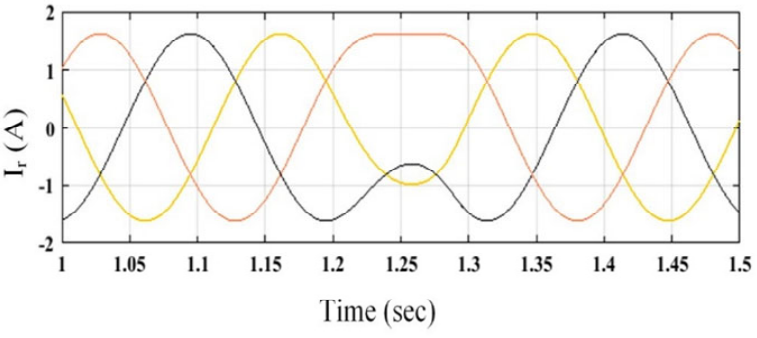

Figure 14 Emulated waveforms of 6-phase DFIG and wind turbine torque for change in wind speed (see online version for colours)

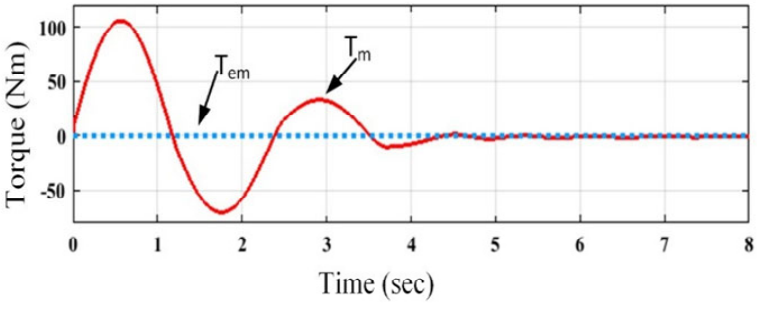

The emulated waveforms of 6-phase DFIG and wind turbine torque for changes in win speed are shown in Figure 14. Since six-phase grid system is not currently commercially available, a six-phase transformer can be used to feed a commercially available three-phase grid system using 6-phase DFIG. The six-phase current and voltage performances can be converted to three-phase parameters after using a six-phase transformer. The voltage and current performance of the six-phase transformer are shown in Figure 15. Figure 15(a) depicts the output voltage of a six-phase transformer, while Figure 15(b) depicts the output current of the six-phase transformer. In addition, 6-phase DFIG's reference speed and mechanical speeds are depicted in Figure 16. Figure 17 depicts the active and reactive power at the grid side. It can be seen that the proposed 6-phase DFIG can feed constant power to the grid even when the wind speed varies. Active and reactive power outputs of 6-phase DFIG are measured as 4 kW and 1,980 Var, respectively.

Figure 15 The application of six-phase transformer for the conversion of six-phase parameters into three-phase parameters for a conventional grid system (a) grid side voltage (b) grid-side current (see online version for colours)

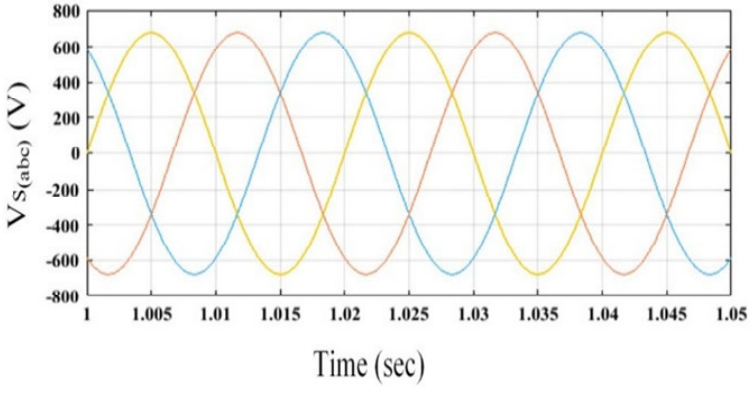

(a)

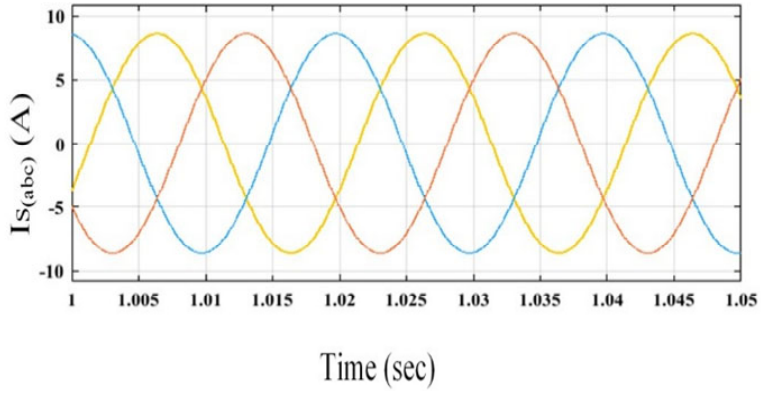

(b)

Figure 16 Emulated speed characteristic of 6-phase DFIG (see online version for colours)

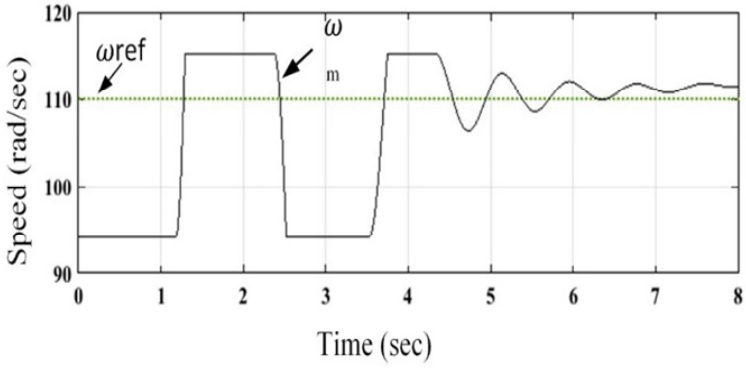

Figure 17 The power build-up characteristics of 6-phase DFIG during speed transition from sub synchronous to super synchronous mode (see online version for colours)

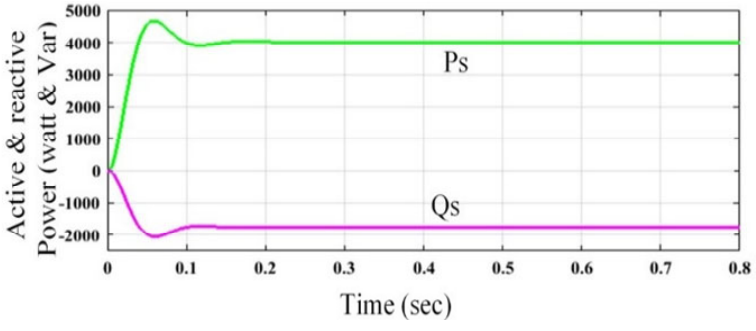

4 Conclusions

The 6-phase DFIG-MPPT Synergy has been developed. The reported 6-phase DFIG-MPPT Synergy will be appropriate for 6-phase DFIG-based wind energy generation system. Moreover this technique will be very helpful for research fraternity if a 6-phase DFIG-based wind energy generation system (WEGS) will supply power to society in future. In addition, the need 6-phase DFIG-based wind energy generation system (WEGS) and modelling of novel 6-phase DFIG, six-phase are accomplished. Furthermore, the performance of WT aerodynamics and 6-phase DFIG are assessed with the DPC-based MPPT strategy. The results and discussion section show that the proposed 6-phase DFIG achieves satisfactory results and a smooth voltage and current waveform under variable wind velocity. The configuration of a 6-phase DFIG ensures stable power during grid feeding. The emulation through OPALRT is performed to validate the effectiveness of the proposed a 6-phase DFIG-based WEGS and the MPPT algorithm. It is found that the proposed 6-phase DFIG-based WEGS provides much better performance while integrating with the real-time grid system.

References

Abad, G., López, J., Rodríguez, M.A., Marroyo, L. and Iwanski, G. (2011) *Doubly Fed Induction Machine: Modeling and Control for Wind Energy Generation*, John Wiley & Sons.

Abdullah, M.A., Yatim, A.H.M., Tan, C.W. and Saidur, R. (2012) 'A review of maximum power point tracking algorithms for wind energy systems', *Renew. Sustain. Energy Rev.*, Vol. 16, No. 5, pp.3220–3227.

Arevalo, J.C., Santos, F. and Rivera, S. (2019) 'Uncertainty cost functions for solar photovoltaic generation, wind energy generation, and plug-in electric vehicles: mathematical expected value and verification by Monte Carlo simulation', *International Journal of Power and Energy Conversion*, Vol. 10, No. 2, pp.171–207.

Bianchi, F.D., De Battista, H. and Mantz, R.J. (2007) *Wind Turbine Control Systems: Principles, Modeling and Gain Scheduling Design*, Vol. 19, Springer, London.

Calderaro, V., Galdi, V., Piccolo, A. and Siano, P. (2008) 'A fuzzy controller for maximum energy extraction from variable speed wind power generation systems', *Electr. Power Syst. Res.*, Vol. 78, No. 6, pp.1109–1118.

Dahri, N., Ouassaid, M. and Yousfi, D. (2023) 'Robust sliding mode hybrid controller applied to a wind energy conversion system based on a doubly-fed induction generator to overcome mechanical parameters uncertainties', *Int. J. Powertrains*, Vol. 12, No. 2, pp.99–123.

Datta, R. and Ranganathan, V.T. (2003) 'A method of tracking the peak power points for a variable speed wind energy conversion system', *IEEE Trans. Energy Convers.*, Vol. 18, No. 1, pp.163–168.

Kazmi, S.M.R., Goto, H., Guo, H-J. and Ichinokura, O. (2010a) 'A novel algorithm for fast and efficient speed-sensorless maximum power point tracking in wind energy conversion systems', *IEEE Trans. Ind. Electron.*, Vol. 58, No. 1, pp.29–36.

Kazmi, S.M.R., Goto, H., Guo, H-J. and Ichinokura, O. (2010b) 'Review and critical analysis of the research papers published till date on maximum power point tracking in wind energy conversion system', *2010 IEEE Energy Conversion Congress and Exposition*, pp.4075–4082.

Khan, M.J. and Mathew, L. (2019a) 'Comparative study of maximum power point tracking techniques for hybrid renewable energy system', *International Journal of Electronics*, Vol. 106, No. 8, pp.1216–1228.

Khan, M.J. and Mathew, L. (2019b) 'Fuzzy logic controller-based MPPT for hybrid photo-voltaic/wind/fuel cell power system', *Neural Comput. Appl.*, Vol. 31, pp.6331–6344.

Koutroulis, E. and Kalaitzakis, K. (2006) 'Design of a maximum power tracking system for wind-energy-conversion applications', *IEEE Transactions on Industrial Electronics*, Vol. 53, No. 2, pp.486–494.

Kumar, D. and Chatterjee, K. (2016) 'A review of conventional and advanced MPPT algorithms for wind energy systems', *Renew. Sustain. Energy Rev.*, Vol. 55, pp.957–970.

Li, H., Shi, K.L. and McLaren, P.G. (2005) 'Neural-network-based sensorless maximum wind energy capture with compensated power coefficient', *IEEE Trans. Ind. Appl.*, Vol. 41, No. 6, pp.1548–1556.

Marques, G.D. and Iacchetti, M.F. (2019) 'DFIG topologies for DC networks: a review on control and design features', *IEEE Transactions on Power Electronics*, Vol. 34, No. 2, pp.1299–1316.

Mishra, N.K. and Husain, Z. (2019) 'Novel six phase doubly fed induction generator through modeling and simulation-a comparison with conventional doubly fed induction generator', *International Conference on Power Electronics, Control and Automation (ICPECA)*, pp.1–5.

Mishra, N.K. and Husain, Z. (2023) 'Application of novel 6-phase doubly fed induction generator for open phases through modeling and simulation', *IETE Journal of Research*, Vol. 69, No. 6, pp.3916–3927.

Mishra, N.K., Husain, Z. and Iqbal, A. (2020) 'Modeling and analysis of novel six-phase DFIG through asymmetrical winding structure for disperse generation', *International Transactions on Electrical Energy Systems*, Vol. 30, No. 12, p.12649.

Mohamed, A.Z., Eskander, M.N. and Ghali, F.A. (2001) 'Fuzzy logic control based maximum power tracking of a wind energy system', *Renew. Energy*, Vol. 23, No. 2, pp.235–245.

Rathi, R. and Sandhu, K.S. (2016) 'Comparative analysis of MPPT algorithms using wind turbines with different dimensions & ratings', *2016 IEEE 1st International Conference on Power Electronics, Intelligent Control and Energy Systems (ICPEICES)*, pp.1–4.

Sridhar, R., Dhar, S. and Dash, S.S. (2015) 'Performance analysis of a stand-alone PV system with reduced switch cascaded multilevel inverter', *International Journal of Power and Energy Conversion*, Vol. 6, No. 2, pp.107–127.

Tiwari, R., Krishnamurthy, K., Neelakandan, R.B., Padmanaban, S. and Wheeler, P.W. (2018) 'Neural network based maximum power point tracking control with quadratic boost converter for PMSG – wind energy conversion system', *Electronics*, Vol. 7, No. 2, p.20.

Yadav, A., Deolia, V.K. and Agrawal, S. (2021) 'Indirect closed-loop control of quasi-Z-source inverter for standalone solar PV-based energy conversion system', *Int. J. Power Energy Convers*., Vol. 12, No. 3, pp.236–251.

Yang, B., Yu, T., Shu, H., Zhang, X., Qu, K. and Jiang, L. (2018) 'Democratic joint operations algorithm for optimal power extraction of PMSG based wind energy conversion system', *Energy Convers. Manag.*, Vol. 159, pp.312–326.

Yang, B., Zhang, X., Yu, T., Shu, H. and Fang, Z. (2017), 'Grouped grey wolf optimizer for maximum power point tracking of doubly-fed induction generator-based wind turbine', *Energy Conversion and Management*, Vol. 133, pp.427–443.